Enhanced linear absorption coefficient of in-plane monolayer graphene on a silicon microring resonator

Heng Cai, Yahui Cheng, He Zhang, Qingzhong Huang, Jinsong Xia, Régis Barille, Yi Wang

Research Article | Vol. 24, No. 21 | 17 Oct 2016 | OPTICS EXPRESS 24105

Optics EXPRESS

Enhanced linear absorption coefficient of *in-plane* monolayer graphene on a silicon microring resonator

HENG CAI,[1] YAHUI CHENG,[1] HE ZHANG,[1] QINGZHONG HUANG,[1] JINSONG XIA,[1] REGIS BARILLE,[2] AND YI WANG[1,*]

[1]*Wuhan National Laboratory for Optoelectronics, Huazhong University of Science and Technology, Wuhan, Hubei 430074, China*

[2]*Moltech Anjou, Université d'Angers/ CNRS UMR 6200, PRES UNAM, 2 bd Lavoisiers, 49045 ANGERS cedex, France*

[*]*ywangwnlo@mail.hust.edu.cn*

Abstract: We demonstrate that enhanced linear absorption coefficient (LAC) of *in-plane* monolayer graphene is determined by the optical transmission spectra of a graphene layer coated symmetrically coupled add-drop silicon microring resonator (SC-ADSMR), of which the value is around 0.23 dB/μm. In contrast to the traditional cut-back method, the measured results aren't dependent on the coupling efficiency between the fiber tip and the waveguide. Moreover, precisely evaluation of graphene layer coated silicon microring resonator (SMR) is crucial for future optoelectronic devices with compact footprint and low power consumption.

OCIS codes: (230.7370) Waveguides; (140.4780) Optical resonators; (310.6860) Thin films, optical properties; (230.3120) Integrated optics devices.

References and links:

1. A. K. Geim and K. S. Novoselov, "The rise of graphene," Nat. Mater. **6**(3), 183–191 (2007).
2. A. K. Geim, "Graphene: status and prospects," Science **324**(5934), 1530–1534 (2009).
3. Y. M. Lin, K. A. Jenkins, A. Valdes-Garcia, J. P. Small, D. B. Farmer, and P. Avouris, "Operation of graphene transistors at gigahertz frequencies," Nano Lett. **9**(1), 422–426 (2009).
4. Q. Bao, H. Zhang, B. Wang, Z. Ni, C. Lim, Y. Wang, D. Tang, and K. P. Loh, "Broadband graphene polarizer," Nat. Photonics **5**(7), 411–415 (2011).
5. F. Wang, Y. Zhang, C. Tian, C. Girit, A. Zettl, M. Crommie, and Y. R. Shen, "Gate-variable optical transitions in graphene," Science **320**(5873), 206–209 (2008).
6. T. Gu, N. Petrone, J. F. McMillan, A. van der Zande, M. Yu, G. Q. Lo, D. L. Kwong, J. Hone, and C. W. Wong, "Regenerative oscillation and four-wave mixing in graphene optoelectronics," Nat. Photonics **6**(8), 554–559 (2012).
7. M. Ji, H. Cai, L. Deng, Y. Huang, Q. Huang, J. Xia, Z. Li, J. Yu, and Y. Wang, "Enhanced parametric frequency conversion in a compact silicon-graphene microring resonator," Opt. Express **23**(14), 18679–18685 (2015).
8. X. Hu, Y. Long, M. Ji, A. Wang, L. Zhu, Z. Ruan, Y. Wang, and J. Wang, "Graphene-silicon microring resonator enhanced all-optical up and down wavelength conversion of QPSK signal," Opt. Express **24**(7), 7168–7177 (2016).
9. Y. Ding, X. Zhu, S. Xiao, H. Hu, L. H. Frandsen, N. A. Mortensen, and K. Yvind, "Effective electro-optical modulation with high extinction ratio by a graphene-silicon microring resonator," Nano Lett. **15**(7), 4393–4400 (2015).
10. L. Yu, J. Zheng, Y. Xu, D. Dai, and S. He, "Local and nonlocal optically induced transparency effects in graphene-silicon hybrid nanophotonic integrated circuits," ACS Nano **8**(11), 11386–11393 (2014).
11. M. Liu, X. Yin, E. Ulin-Avila, B. Geng, T. Zentgraf, L. Ju, F. Wang, and X. Zhang, "A graphene-based broadband optical modulator," Nature **474**(7349), 64–67 (2011).
12. C. Y. Wong, Z. Cheng, Z. Shi, Y. M. Chen, K. Xu, and H. K. Tsang, "Mode-locked fiber laser using graphene on silicon waveguide," in *Proceedings of 10th International Conference on Group IV Photonics (GFP)* (IEEE 2013), pp. 35–36.
13. A. Pospischil, M. Humer, M. M. Furchi, D. Bachmann, R. Guider, T. Fromherz, and T. Mueller, "CMOS-compatible graphene photodetector covering all optical communication bands," Nat. Photonics **7**(11), 892–896 (2013).
14. X. Gan, R.-J. Shiue, Y. Gao, I. Meric, T. F. Heinz, K. Shepard, J. Hone, S. Assefa, and D. Englund, "Chip-integrated ultrafast graphene photodetector with high responsivity," Nat. Photonics **7**(11), 883–887 (2013).

#273287 http://dx.doi.org/10.1364/OE.24.024105
Journal © 2016 Received 8 Aug 2016; revised 5 Oct 2016; accepted 6 Oct 2016; published 10 Oct 2016

Optics EXPRESS

15. W. Bogaerts, P. De Heyn, T. Van Vaerenbergh, K. De Vos, S. K. Selvaraja, T. Claes, P. Dumon, P. Bienstman, D. Van Thourhout, and R. Baets, "Silicon microring resonators," Laser Photonics Rev. **6**(1), 47–73 (2012).
16. M. S. Ünlü and S. Strite, "Resonant cavity enhanced photonic devices," J. Appl. Phys. **78**(2), 607–639 (1995).
17. H. Zhou, T. Gu, J. F. McMillan, M. Yu, G. Lo, D.-L. Kwong, G. Feng, S. Zhou, and C. W. Wong, "Enhanced photoresponsivity in graphene-silicon slow-light photonic crystal waveguides," Appl. Phys. Lett. **108**(11), 111106 (2016).
18. M. Mohsin, D. Schall, M. Otto, A. Noculak, D. Neumaier, and H. Kurz, "Graphene based low insertion loss electro-absorption modulator on SOI waveguide," Opt. Express **22**(12), 15292–15297 (2014).
19. C. Horvath, D. Bachman, G. Mi, and V. Van, "Fabrication and characterization of edge-conformed graphene-silicon waveguides," IEEE Photonics Technol. Lett. **27**(6), 585–587 (2015).
20. H. Li, Y. Anugrah, S. J. Koester, and M. Li, "Optical absorption in graphene integrated on silicon waveguides," Appl. Phys. Lett. **101**(11), 111110 (2012).
21. R. Kou, S. Tanabe, T. Tsuchizawa, K. Warabi, S. Suzuki, H. Hibino, H. Nakajima, and K. Yamada, "Characterization of optical absorption and polarization dependence of single-layer graphene integrated on a silicon wire waveguide," Jpn. J. Appl. Phys. **52**(6R), 060203 (2013).
22. L. Yu, Y. Xu, Y. Shi, and D. Dai, "Linear and nonlinear optical absorption of on-chip silicon-on-insulator nanowires with graphene," in *Proceedings of Asia Communications and Photonics Conference* (Optical Society of America, 2012), pp. AS1B–3.
23. G. Kovacevic and S. Yamashita, "Waveguide design parameters impact on absorption in graphene coated silicon photonic integrated circuits," Opt. Express **24**(4), 3584–3591 (2016).
24. S. Xiao, M. H. Khan, H. Shen, and M. Qi, "Modeling and measurement of losses in silicon-on-insulator resonators and bends," Opt. Express **15**(17), 10553–10561 (2007).
25. C. C. Evans, C. Liu, and J. Suntivich, "Low-loss titanium dioxide waveguides and resonators using a dielectric lift-off fabrication process," Opt. Express **23**(9), 11160–11169 (2015).
26. A. Das, S. Pisana, B. Chakraborty, S. Piscanec, S. K. Saha, U. V. Waghmare, K. S. Novoselov, H. R. Krishnamurthy, A. K. Geim, A. C. Ferrari, and A. K. Sood, "Monitoring dopants by Raman scattering in an electrochemically top-gated graphene transistor," Nat. Nanotechnol. **3**(4), 210–215 (2008).
27. V. Van, T. Ibrahim, P. Absil, F. Johnson, R. Grover, and P.-T. Ho, "Optical signal processing using nonlinear semiconductor microring resonators," IEEE J. Sel. Top. Quantum Electron. **8**(3), 705–713 (2002).
28. R. Kou, S. Tanabe, T. Tsuchizawa, T. Yamamoto, H. Hibino, H. Nakajima, and K. Yamada, "Influence of graphene on quality factor variation in a silicon ring resonator," Appl. Phys. Lett. **104**(9), 091122 (2014).
29. T. Gu, H. Zhou, J. F. McMillan, N. Petrone, A. van der Zande, J. C. Hone, M. Yu, G.-Q. Lo, D.-L. Kwong, and C. W. Wong, "Coherent four-wave mixing on hybrid graphene-silicon photonic crystals," IEEE J. Sel. Top. Quantum Electron. **20**(1), 7500106 (2014).
30. I. F. Crowe, N. Clark, S. Hussein, B. Towlson, E. Whittaker, M. M. Milosevic, F. Y. Gardes, G. Z. Mashanovich, M. P. Halsall, and A. Vijayaraghaven, "Determination of the quasi-TE mode (in-plane) graphene linear absorption coefficient via integration with silicon-on-insulator racetrack cavity resonators," Opt. Express **22**(15), 18625–18632 (2014).
31. X. Gan, K. F. Mak, Y. Gao, Y. You, F. Hatami, J. Hone, T. F. Heinz, and D. Englund, "Strong enhancement of light-matter interaction in graphene coupled to a photonic crystal nanocavity," Nano Lett. **12**(11), 5626–5631 (2012).
32. D. Chatzidimitriou, A. Pitilakis, and E. E. Kriezis, "Rigorous calculation of nonlinear parameters in graphene-comprising waveguides," J. Appl. Phys. **118**(2), 023105 (2015).
33. P.-Y. Chen and A. Alù, "Atomically thin surface cloak using graphene monolayers," ACS Nano **5**(7), 5855–5863 (2011).
34. V. Sorianello, M. Midrio, and M. Romagnoli, "Design optimization of single and double layer Graphene phase modulators in SOI," Opt. Express **23**(5), 6478–6490 (2015).

1. Introduction

Graphene is a two-dimensional material [1,2], which exhibits remarkable optoelectronic characteristics, such as ultrahigh carrier mobility at room temperature [3], ultra-broadband absorption [4], controllable band-gap transition [5], and giant Kerr coefficient [6]. Graphene has been integrated on photonic integrated circuits (PICs) in which the hexagonal carbon sheet is evanescently coupled to the waveguide, leading to unprecedented optical performances [7–10].

Recently, graphene resting on silicon-on-insulator (SOI) platform offers great potential for optoelectronic devices. Broadband optical modulators [11], mode locked laser [12] and high-responsivity photodetectors [13, 14] have all been demonstrated utilizing graphene-silicon hybrid waveguides (GSHWs). However, these non-resonant structures adopting straight waveguides require large-area graphene, which range from several tens to several hundred micrometers, to obtain sufficient optical absorption, resulting in large footprint and high

Optics EXPRESS

power consumption. Owing to its intrinsic field enhancement (FE), silicon microring resonators (SMRs) [15] can strengthen the light-matter interaction, which is promising in reduction of footprint and power consumption by the GSHWs. Thus, monolithic integration of graphene on SMRs offer great opportunities in resonant cavity enhanced photonic devices [16], which is beneficial to photodetectors [17], optical modulators [18] and mode-locked lasers [12].

The fundamental feature in GSHWs is the optical absorption property of graphene [18]. Consequently, precisely evaluation of linear absorption coefficients (LACs) would be an important task in optimizing optical performances of the proposed GSHWs. Even though the LACs of GSHWs have been measured ranging from 0.03 dB/μm to 0.2 dB/μm for TE mode [19, 20] while 0.05 dB/μm to 0.33 dB/μm for TM mode [21, 22], the unique absorption properties in this configuration are still to be fully characterized, theoretically or experimentally, as mentioned in [23]. In previous reports, the LACs of GSHWs were generally obtained through a cut-back method [9, 10]. However this method is subject to several problems, for instance,

(i). The coupling efficiencies between the fiber tips and the waveguides as well as waveguide end facets maintain non-uniformity. Moreover, fiber-to-waveguide coupling losses are often comparable to or even much higher than the propagation losses in the waveguides [20, 22], leading to high uncertainties in loss measurements, as stated in [24].

(ii). The measured losses in these straight hybrid waveguides deviate from linear fit when the lengths of the transferred graphene are beyond 500 μm because of coverage problems, which is a fairly common situation [9].

(iii). This widely used method could not be directly applied to the measurement of resonant-enhanced optical absorption, which has not been measured and fully understood in the literature.

In this paper, we present a comprehensive method to determine the enhanced LAC of *in-plane* monolayer graphene on a microring resonator, on which graphene with only several micrometers in length is used. Commercially available monolayer graphene grown by chemical vapor deposition (CVD) is transferred onto the fabricated symmetrical add-drop SMR. The monolayer graphene patterning is accomplished by an electron beam lithography (EBL) process following by a "lift-off" process. Simulation results based on Finite Element Method (FEM) show that enhanced optical absorptions of monolayer graphene on our resonator are two times larger than those of monolayer graphene on silicon straight waveguide, which is in accordance with our experimental measurements. The enhanced absorption of *in-plane* monolayer graphene is wavelength-independent in the telecommunication band, which could be explained by the unique band structure of monolayer graphene [1,2]. More importantly, enhanced optical absorption with equally wavelength spacing can be potentially applied in resonance-enhanced photodetectors for chip-scale wavelength-division multiplexed optical interconnects.

2. Experimental details

A symmetrically coupled add-drop silicon microring resonator (SC-ADSMR) consisting of a SMR and dual stripe waveguides working as through and drop ports is fabricated. The SMR has a width of W = 500 nm, a height of H = 220 nm and a radius of R = 15 μm, which is fabricated on a SOI wafer with a buried oxide (BOX) layer of 3 μm using EBL and inductively coupled plasmon (ICP) etching. The stripe waveguides are laterally coupled with the SMR and both of them have the same dimensions. The corresponding gaps between the stripes and SMR are 125 nm and 117 nm respectively. The nearly identical gaps show that the fabricated add-drop silicon microring resonator is symmetrically coupled.

Optics EXPRESS

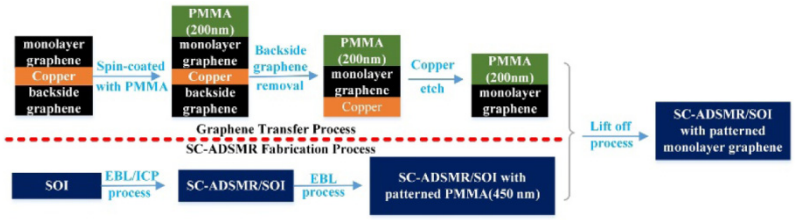

Fig. 1. The processes of monolayer graphene preparation and SC-ADSMR device fabrication.

Figure 1 illustrates the monolayer graphene transfer and SC-ADSMR device fabrication processes. The CVD monolayer graphene is grown on both sides of a copper foil (Cu) in a first step. A 200-nm thick poly (methyl methacrylate) (PMMA) (Allresist, AR-P 672.045) film is spin-coated onto the upper surface of layered backside graphene/Cu/monolayer graphene to protect monolayer graphene from damage in a second step. The sample consisting of layered backside graphene/Cu/monolayer graphene/PMMA is floated on marble's etchant with 15 grams of copper(II) sulfate pentahydrate ($CuSO4{\cdot}5H2O$), 50 ml of deionized water (DI), and 50 ml of concentrated hydrochloric acid (HCl). The backside graphene is totally removed after 2-min of chemical etching. Then the Cu/monolayer graphene/PMMA sample is floated on DI for about 3 minutes to remove the chemical impurities. Another marble's etchant with the same chemical recipe is applied for removing the Cu beneath monolayer graphene. The etching time is about 1.5 hours. The remained sample consisting of a layered monolayer graphene/PMMA is last rinsed in DI, leaving it ready for transferring. We employ the following processes to transfer monolayer graphene to a specific region of the SC-ADSMR by ripping out the abundant monolayer graphene: a 450-nm thick PMMA film is spin-coated onto the SOI wafer containing fabricated SC-ADSMR device and a specific region with a 45 degree sector area is patterned using EBL, followed by developing and fixing of the PMMA photoresist. In the time, the prepared monolayer graphene/PMMA sample is transferred onto the chip followed by drying with a mild nitrogen blow. Subsequently, a "lift-off" process is introduced to form the monolayer graphene coated SC-ADSMR device. The whole chip is baked at 180°C for 15 minutes. The PMMA is then dissolved in hot acetone for about 1 hour. The removal of PMMA also results in cutting-away of monolayer graphene resting on the 450-nm thick PMMA, which is similar to a lift-off [22, 25] process. Finally, the chip is rinsed with isopropyl alcohol (IPA) for further cleaning and then dried again by a mild nitrogen blow. A scanning electron micrograph (SEM) picture of the monolayer graphene coated SC-ADSMR device with partial part of the stripe waveguides is shown in Fig. 2(a), where secondary-electron contrast is obtained. The possible reason for imaging contrast lies in different secondary-electron-generation efficiencies of silicon, silicon oxide and monolayer graphene. At the boundary of patterned monolayer graphene, the random roughness of monolayer graphene is large due to the coarse-controlled "lift-off" process.

The detailed SEM picture of our fabricated GSHW is shown in Fig. 2(b), in which the patterned top-monolayer-graphene rests on the surface of the waveguide and side-monolayer-graphene extends to the surface of BOX layer, forming a trapezoid configuration. According to our measurements, the radial length of side-monolayer-graphene is estimated as X = 200 nm. Figure 2(c) shows the photonic crystal grating coupler, which is optimized for TE mode coupling exhibiting an insertion loss of 7.5 dB per facet.

Optics EXPRESS

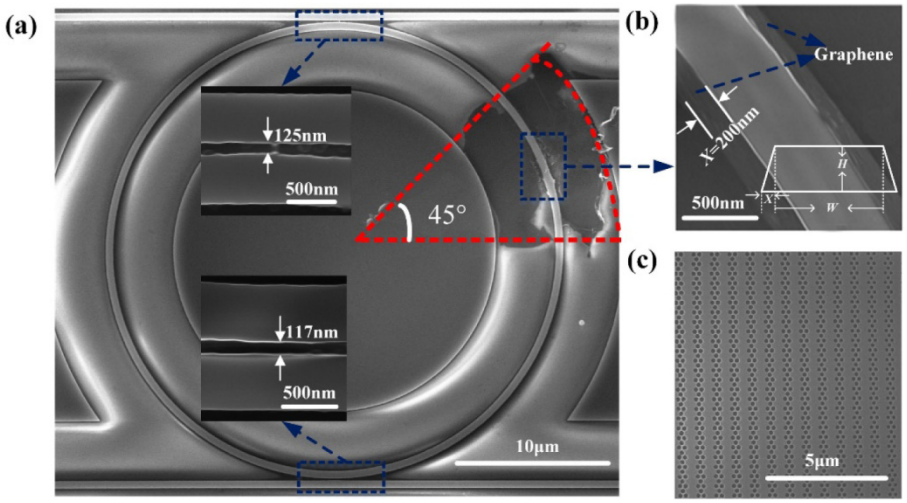

Fig. 2. (a) SEM image of the SC-ADSMR covered with patterned monolayer graphene (top view). Close-up view of the two coupling regions are also shown. (b) Zoom-in SEM images of the local monolayer graphene covered area in (a), showing that monolayer graphene uniformly clings to the silicon waveguide. Here X is the radial length of side-monolayer-graphene and W is the width of waveguide. (c) Photonic crystal grating coupler used for coupling light into and out of the SC-ADSMR device.

Adopting the experimental setup in Fig. 3(a), the SC-ADSMR is characterized by an amplified spontaneous emission (ASE) light source (Amonics, AEDFA-300-B-FA) ranging from 1535 nm to 1565 nm. The normalized transmission spectra of through port before and after monolayer graphene transfer (noted as woGr and wGr respectively) are recorded by an optical spectrum analyzer (OSA, YOKOGAWA AQ6370), which is shown in Fig. 3(b). It shows that the resonator before and after monolayer graphene transfer have a mean free spectral range (FSR) of FSR = 5.74 nm. The significant reduction of extinction ratio and broadening of the resonances in Fig. 3(b) are the result of increased propagation loss (absorption) induced by monolayer graphene. The red shift of resonances is probably a result of the change in the mode effective refractive index induced after transfer of the graphene.

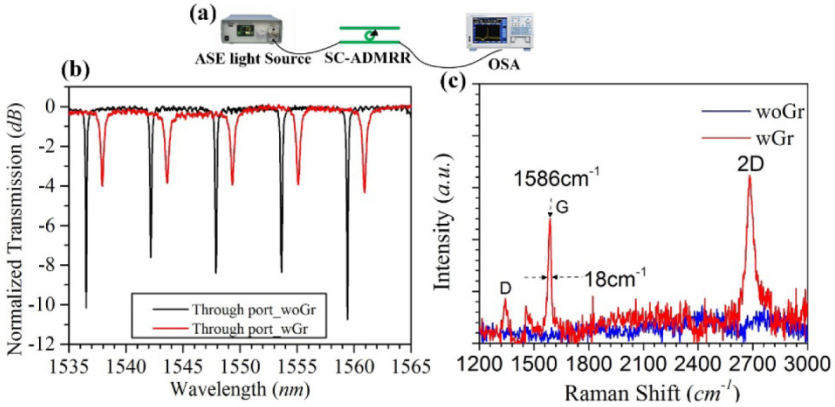

Fig. 3. (a) Experimental setup for characterizing the LAC of *in-plane* graphene. (b) Optical transmission spectra of the SC-ADSMR device before and after monolayer graphene transfer (noted as woGr and wGr respectively). (c) Raman spectra measured in the graphene-covered region (red) and in the area where graphene is lifted off (blue).

Optics EXPRESS

The explicit characterization of monolayer graphene is obtained by Raman spectrum. In Fig. 3(c), we have measured Raman spectrum of the graphene layer coated SC-ADSMR device using a spectrometer with high resolution (LabRAM HR800, France, Jobin Yvon). The blue curve represents Raman spectrum of the area where graphene is lifted off and we see that the typical Raman peaks are missing. The red curve shows a G peak (~1586 cm^{-1}) with a full width at half maximum (FWHM) of ~18 cm^{-1} and a 2D peak (~2700 cm^{-1}), with a 2D-to-G peak intensity ratio of about 1.2, implying that the transferred graphene is a monolayer and the corresponding chemical potential is around 0.2 eV [26]. Moreover, a weak D peak is also found at ~1350 cm^{-1}, indicating the transferred monolayer graphene is of high quality. We have also measured the Raman spectra in some other regions. The results turn out to be similar to the Raman spectra presented in Fig. 3(c).

3. Experimental Results

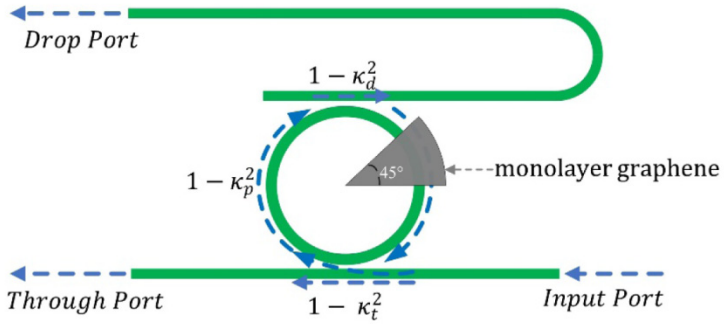

Fig. 4. Scheme of the SC-ADSMR with patterned monolayer graphene

We have adopted an analytical model proposed by Shijun Xiao *et al*. [24] to characterize the propagation loss in our monolayer graphene covered SC-ADSMR device. In Fig. 4, schematic diagram of the model is presented. κ_t^2, κ_d^2 are coefficients representing the fraction of optical power coupled into and out of the SMR through input and drop port respectively. κ_p^2 is the fraction of optical power losses per round-trip in the SMR due to intrinsic losses mainly resulting from graphene absorption and roughness induced scattering. In our case, $\kappa_t = \kappa_d$ is satisfied and the optical response of through port is given as [24]:

$$T_{through}(\lambda) = \frac{(\lambda-\lambda_0)^2 + \left(\frac{FSR}{4\pi}\right)^2 (\kappa_p^2)^2}{(\lambda-\lambda_0)^2 + \left(\frac{FWHM_t}{2}\right)^2}. \quad (1)$$

where $T_{through}(\lambda)$ is the power transmission of through port, $FWHM_t$ is the FWHM of the optical transmission spectrum at the through port and λ_0 is the resonant wavelength. When the input wavelength is at resonance ($\lambda = \lambda_0$), $T_{through}(\lambda)$ has a minimal value of γ_t satisfying:

$$ER_t(dB) = -10\log_{10}(\gamma_t). \quad (2)$$

with ER_t and γ_t the extinction ratio and minimal power transmission at the through port respectively. The coefficients κ_t, κ_d and κ_p are described as:

Optics EXPRESS

$$\kappa_{\mathrm{p}}^2 = \frac{2\pi FWHM_t\sqrt{\gamma_t}}{FSR}, \tag{3}$$

$$\kappa_{\mathrm{t}}^2 = \kappa_d^2 = \frac{\pi FWHM_t\left(1-\sqrt{\gamma_t}\right)}{FSR}, \tag{4}$$

The loss per round-trip in the resonator is determined by:

$$\alpha\left(dB/round\right) = -10\log_{10}\left(1-\kappa_p^2\right). \tag{5}$$

Also, the Q factor, Finesse and FE of the SC-ADSMR are summarized as [15,27]:

$$Q = \frac{\lambda_0}{FWHM_t}, \tag{6}$$

$$Finesse = \frac{FSR}{FWHM_t} = \frac{2\pi}{\kappa_t^2+\kappa_d^2+\kappa_p^2}, \tag{7}$$

$$FE = \sqrt{\frac{Finesse}{\pi}}. \tag{8}$$

In the proposed device, an eighth part of the resonator is covered with monolayer graphene. The total losses of SMR coated with monolayer graphene include the linear absorption (LA) of *in-plane* monolayer graphene and LA of silicon waveguide. Assuming graphene "lift off" process does not induce extra LA in the silicon waveguide, the LAC of silicon waveguide and GSHW can be written as:

$$LAC_{silicon} = \frac{\alpha_{woGr}}{2\pi R}, \tag{9}$$

$$LAC_{GSHW} = \frac{(\alpha_{wGr}-\alpha_{woGr}(1-n))}{2\pi nR}. \tag{10}$$

where α_{woGr} and α_{wGr} correspond to the loss per round-trip before and after graphene transfer respectively, n = 1/8 corresponds to the fractional coverage length of monolayer graphene. Thus, the LAC of *in-plane* monolayer graphene on the silicon microring resonator is expressed as:

$$LAC_{Gr\_resonator} = LAC_{GSHW} - LAC_{silicon}. \tag{11}$$

Table 1 shows detailed experimental results before and after graphene transfer, including the resonant wavelengths, the corresponding extinction ratio and FWHM of transmission spectra. By using the analytical method mentioned above, the enhanced LAC of *in-plane* monolayer graphene in our case is nearly identical, of which the mean value is ~0.23 dB/μm.

Optics EXPRESS

Table 1. Parameters for LAC deduction before and after graphene transfer.

Deduced Parameters before and after graphene transfer (noted as woGr and wGr respectively)						
Resonance	w/o Gr	λ_1	λ_2	λ_3	λ_4	λ_5
	woGr	1536.52	1542.19	1547.90	1553.65	1559.42
	wGr	1537.94	1543.62	1549.34	1555.10	1560.90
ER_t (dB)	woGr	9.89	8.18	8.84	9.01	10.78
	wGr	3.79	3.56	3.70	3.97	4.23
$FWHM_t$ (nm)	woGr	0.17	0.225	0.221	0.231	0.207
	wGr	0.375	0.433	0.405	0.450	0.424
Calculated Parameters before and after graphene transfer (noted as woGr and wGr respectively)						
$\kappa_e^2 = \kappa_d^2$	woGr	0.0632	0.0751	0.0772	0.0817	0.0805
	wGr	0.0726	0.0797	0.0769	0.0905	0.0895
κ_p^2	woGr	0.0597	0.0960	0.0874	0.0897	0.0655
	wGr	0.2654	0.3146	0.2895	0.3119	0.2851
Q factor	woGr	9038	6854	7004	6726	7533
	wGr	4101	3565	3826	3456	3681
Finesse	woGr	33.7624	25.5207	25.9851	24.8249	27.7403
	wGr	15.3024	13.2557	14.1737	12.7474	13.5384
FE	woGr	3.2782	2.8502	2.8760	2.8111	2.9715
	wGr	2.2070	2.0541	2.1241	2.0144	2.0759
$LAC_{Gr\_resonator}$	wGr	0.21 dB/μm	0.24 dB/μm	0.21 dB/μm	0.24 dB/μm	0.23 dB/μm
	mean value	0.23 dB/μm				

Given the fact that in most previously published works [21, 28–30] the LACs of monolayer graphene on silicon waveguides have a typical value of ~0.1 dB/μm, which are one time smaller than the LACs in our case. The difference can be explained by the field enhancement in our SC-ADSMR device which lies in enhancement in the interaction of light with graphene through coupling resonant modes within the silicon microring resonator [31]. To fully understand this discrepancy, we introduce FE parameter and the sidewall loss in the next section to simulate the propagation loss of our fabricated device.

4. Simulation Model and Discussion

Most widely used method for simulating graphene in literature is the equivalent bulk medium approach, in which graphene is modeled as a bulk-material layer of finite thickness [9]. However, the simulation results with this approach are strongly dependent on the simulated grid size and the thickness of monolayer graphene, which leads to inefficient calculation. Hence, we model the atomic-thick layer as a conductive surface in a commercial software (COMSOL Multiphysics) according to its fundamental optical properties and boundary conditions, which has been approved valid and more efficient [23, 32].

Graphene can be treated electromagnetically by its surface dynamic conductivity in a complex form consisting of interband and intraband contributions [33]:

$$\sigma(\omega,\mu_c,\tau,T)=\sigma_{\text{int}ra}(\omega,\mu_c,\tau,T)+\sigma_{\text{int}er}(\omega,\mu_c,\tau,T). \tag{12}$$

The intraband contribution can be evaluated as:

$$\sigma_{\text{int}ra}(\omega,\mu_c,\tau,T)=i\frac{e^2k_BT}{\pi\hbar^2(\omega+i\tau^{-1})}\left[\frac{|\mu_c|}{k_BT}+2In\left(\exp\left(-\frac{|\mu_c|}{k_BT}\right)+1\right)\right]. \tag{13}$$

For $\hbar\omega$ and $|\mu_c|$ □ k_BT, the interband contribution is expressed as:

Optics EXPRESS

$$\sigma_{inter}(\omega,\mu_c,\tau,T)=i\frac{e^2}{4\pi\hbar}In\left[\frac{2|\mu_c|-\hbar(\omega+i\tau^{-1})}{2|\mu_c|+\hbar(\omega+i\tau^{-1})}\right]. \quad (14)$$

where e is the electron charge, k_B is the Boltzmann constant, ħ is the reduced Planck's constant, ω is the angular frequency of incident light, T is the temperature, μ_c is the chemical potential and τ is the momentum relaxation of carriers in monolayer graphene. Adopting an incident wavelength of λ_s = 1550 nm, a temperature of T = 300 K and a momentum relaxation of τ = 12 fs [34], σ (ω, μ_c, τ, T) is numerically calculated and plotted as a function of graphene's chemical potential in Fig. 5.

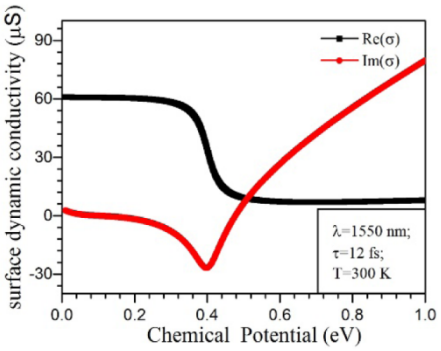

Fig. 5. Surface dynamic conductivity of monolayer graphene as a function of its chemical potential

The optical linear absorption of graphene is directly determined by the real part of its surface dynamic conductivity shown in Fig. 5. Thus Eqs. (12), (13) and (14) are implemented in COMSOL Multiphysics and the enhanced LAC of *in-plane* monolayer graphene in our SC-ADSMR device is modelled with a 2D configuration illustrated in Fig. 6(a), in which the graphene locates on top of the silicon waveguide and attaches to the BOX layer at an angle of φ with respect to the side wall of silicon waveguide. According to our estimation through SEM picture (section 2), *X* has a value of ~200 nm in experiment. The corresponding surface current density of monolayer graphene in Fig. 6(a) is expressed as [23, 32]:

$$\mathbf{J}_{//}=\sigma(\omega,\mu_c,\tau,T)\cdot(FE\cdot\mathbf{E}_{//}), \quad (15)$$

$$\mathbf{J}_{\perp}=0. \quad (16)$$

where subscript // and ⊥ denote the field component that is tangential and normal to the graphene sheet, respectively, **E** is the electrical field and **J** is the surface current density of monolayer graphene. Equation (15) given by Ohm's law is critical, in which the FE of silicon microring resonator is taken into consideration, because the enhanced optical absorption of graphene-on-resonator mainly origins from the localized electrical field in our resonator. FE is deliberately solved *via* Eqs. (7) and (8) and presented in Table 1 (section 3). Because electric fields perpendicular to the surface of silicon microring have no interaction with monolayer graphene, the corresponding surface current density in the perpendicular direction could be set as zero as written in Eq. (16). In the simulation, a mesh size of 1 nm is chosen for monolayer graphene and a chemical potential of ~0.2 eV is confirmed by the Raman spectrum, which is also identical to the reported values of PMMA-transferred monolayer graphene [20]. With these parameters, the complex effective refractive index of GSHW in Fig. 6(a) is calculated in COMSOL Multiphysics. Then, the LAC of *in-plane* monolayer graphene in the proposed structure is obtained through [9]:

Optics EXPRESS

$$\alpha(dB/\mu m) = 2k_0 n_{eff,imag} \times 4.343 \times 10^{-6}. \quad (17)$$

where k_0 is the vacuum wave number, subscript *imag* denotes the imaginary part of modal effective index and 4.343×10^{-6} is the constant for converting from m^{-1} to dB/μm. Figure 6(b) shows that the enhanced LAC of *in-plane* monolayer graphene in our case has an average value of ~0.20 dB/μm in simulation, which agrees well with the experimental results (~0.23 dB/μm).

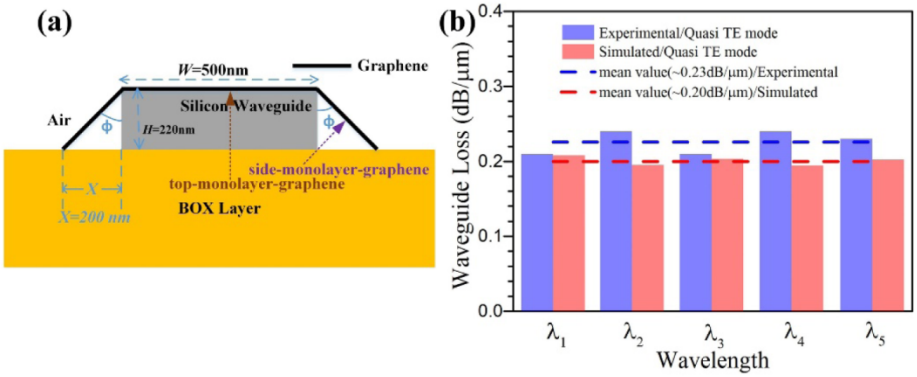

Fig. 6. (a) Cross section of the simulated GSHW. (b) Experimental and simulated LAC of *in-plane* monolayer graphene as a function of the five resonant wavelengths of our SC-ADSMR device. In this simulation, the FEs of the SC-ADSMR and side-monolayer-graphene which is clung to the waveguide have both been taken into consideration. Here, λ_1 = 1537.94 nm, λ_2 = 1543.62 nm, λ_3 = 1549.34 nm, λ_4 = 1555.10 nm and λ_5 = 1560.90 nm represent the five resonant wavelengths of our SC-ADSMR device after graphene transfer process.

The parameter of *X* is estimated through SEM picture from top view (section 2), which possibly leads to inaccuracy of optical absorption. In order to verify our theoretical model with experimental results, we further simulated the enhanced LAC of *in-plane* monolayer graphene for quasi TE mode based on our SC-ADSMR device with a varying *X* parameter. By fixing FE to an average value of ~2.10, x, y and z component of electric field at the incident wavelength of 1550 nm is shown in Fig. 7(a). Mesh grids of our device are also presented, in which the densest grids indicate where monolayer graphene is located. In the top of Fig. 7(a), the x-component of electric field of the GSHW is evanescently coupled with top-monolayer-graphene and side-monolayer-graphene. In the middle of Fig. 7(a), y-component of electric field of the GSHW can't contribute to the optical absorption owing to Eq. (16). Interestingly, the z-component of electric field in GSHW strongly interacts with the side-monolayer-graphene, which is often neglected in the literature [19, 20]. Following the electric fields distribution in Fig. 7(a), the LAC of GSHW is plotted as a function of parameter *X* in Fig. 7(b). For fundamental quasi TE mode in our case, LA of GSHW origins from both the side-monolayer-graphene and top-monolayer-graphene. With the parameter of *X* = 200 nm, the optical absorption by top-monolayer-graphene is ~0.15 dB/μm, while the corresponding contribution by side-monolayer-graphene is ~0.05 dB/μm, which can't be neglected in resonant configuration. With increased parameter of *X* (*X*>200 nm), the coupling between electric field of GSHW and side-monolayer-graphene becomes weaker, resulting in small variation of optical absorption (~0.01 dB/μm). It is worth noting that when *X*>100 nm, the fluctuation of our simulated LACs will never exceed ± 0.01 dB/μm compared to the simulated result at *X* = 200 nm, which indicate that the experimental results fit well with the simulation.

Optics EXPRESS

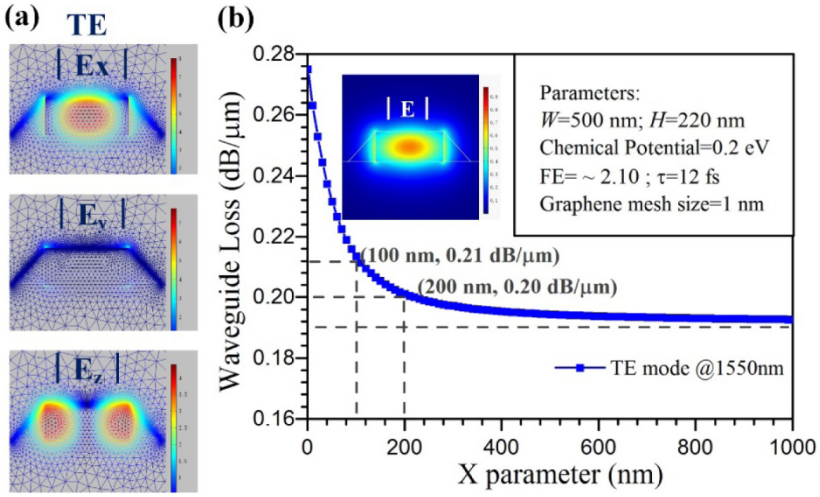

Fig. 7. (a) The x, y and z components of electrical field in the GSHW. Here the mesh grids are also shown. (b) The LAC of GSHW in Fig. 6(a) with a varying parameter of *X*. The inset shows typical fundamental quasi TE mode profile of simulated GSHW at 1550 nm. Other parameters for this simulation are also shown in the box above.

The simulation results (~0.20 dB/μm) are slightly lower than the experimental ones (~0.23 dB/μm). The small discrepancy is attributed to the following facts:

(i). The "lift-off" procedures cause wrapping of graphene at the edges which lead to light scattering when light enters the waveguide section covered with graphene.

(ii). The surface roughness of silicon waveguide or Cu residues also introduce extra loss.

Furthermore, we also estimate the absorption case for TM mode, which is illustrated in Fig. 8.

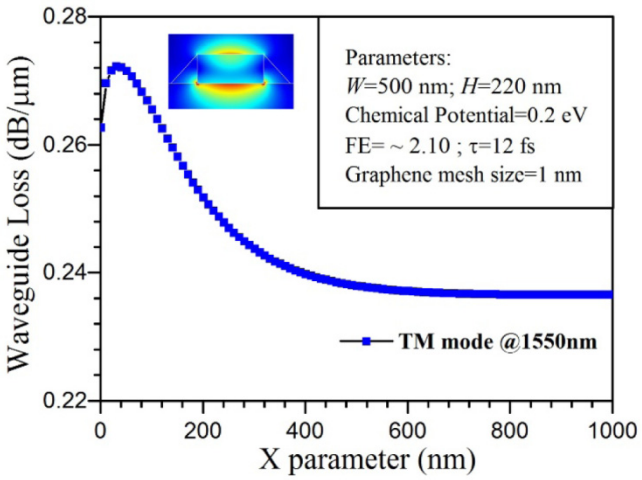

Fig. 8. Simulated waveguide loss for TM mode as a function of parameter X.

The absorption of TM mode is larger than that of TE mode when X>10 nm. This is attributed to tangential component of the localized electric field.

Optics EXPRESS

5. Conclusion

We propose a comprehensive way towards direct determination of the LACs of *in-plane* monolayer graphene integrated with a SC-ADSMR device, which does not depend on the coupling efficiencies between the fiber tips and the waveguides as well as the waveguide end facets. A SC-ADSMR with patterned monolayer graphene is designed and fabricated, in which the universal enhanced LAC of *in-plane* monolayer graphene over a large wavelength range is proportional to the field enhancement in SMR. Our work provides an efficient method to evaluate the linear optical performances of high-performance graphene-comprising waveguides leading to compact-footprint and low-power-consumption PICs.

Funding

National Basic Research Program of China (Grant No. 2012CB922103 and 2013CB933303); National Scientific Founding of China (Grant No. 60806016 and 61177049).

Acknowledgments

We thank all the engineers in the Center of Micro-Fabrication and Characterization (CMCF) of Wuhan National Laboratory for Optoelectronics (WNLO) for the support in device fabrication.